Journal of Power Sources 266 (2014) 464–470

Contents lists available at ScienceDirect

Journal of Power Sources

journal homepage: www.elsevier.com/locate/jpowsour

Metal sulfide counter electrodes for dye-sensitized solar cells: A balanced strategy for optical transparency and electrochemical activity

J. Song, G.R. Li*, C.Y. Wu, X.P. Gao*

Institute of New Energy Material Chemistry, Collaborative Innovation Center of Chemical Science and Engineering (Tianjin), Tianjin Key Laboratory of Metal and Molecule Based Material Chemistry, Nankai University, Tianjin 300071, China

HIGHLIGHTS

- Group VIIIB metal sulfides thin films are prepared by a solution-process strategy.
- The sulfide electrodes achieve optical transparency and high electrochemical activity.
- The DSSC using nickel sulfide shows a higher efficiency than using Pt electrode.

ARTICLE INFO

Article history:
Received 24 February 2014
Received in revised form
8 May 2014
Accepted 12 May 2014
Available online 21 May 2014

Keywords:
Solar cells
Counter electrodes
Metal sulfides
Electrocatalysis
Optical transparency

ABSTRACT

Dye-sensitized solar cells (DSSCs) have obtained exciting progress in improving energy conversion efficiency and cutting material cost in recent years. It is found that many kinds of inorganic compounds have promising potential to replace platinum as counter electrode materials for DSSCs. Actually, to a thin film electrode, preparation of the thin film is the same important as choice of active materials, because quality of the films has a direct effect on electrochemical and optical performance of the final counter electrodes. In this paper, a general strategy is developed to prepare transparent and high-efficient metal sulfide counter electrodes. In the route, the Group VIIIB metal sulfides are formed as compact, homogenous and stable films on fluorine-doped tin oxide conductive glass from a precursor organic solution by spin coating, and the film thickness can be readily converted to reach the balance between optical transparency and electrochemical activity. Among the Group VIIIB metal sulfides, the nickel sulfide film with the thickness of 100 nm shows the high transparency and energy conversion efficiency of 7.37%, higher than that of the DSSC using platinum electrode. The results provide a new and facile alternative to prepare high-efficient and transparent sulfide counter electrodes for DSSCs.

1. Introduction

Transparency is one of the most attractive features of dye-sensitized solar cells (DSSCs), distinguished from silicon-based solar cells [1,2]. Transparent or translucent solar cells can be used as window glasses, curtain walls, and indoor ornamentals to construct energy-balanced architectures in future [1–5]. It has also been confirmed that energy conversion efficiency of the transparent devices can be obviously improved with a reflecting mirror behind [6,7]. To fabricate a transparent DSSC, a popular counter electrode is platinum filmed on conductive glass [1–6]. Though platinum answers for the functional requirements of counter electrodes, such as excellent electrical conductivity, high electrocatalytic activity and good transparency, researchers are struggling to seek for low-cost substitutes for the expensive and scarce metal [8–10]. It has been found that some carbon allotropes such as nanosized carbon [11], graphite [12], graphene-based hybrid [13], mesoporous carbon [14–17] and carbon fibers [18,19], conducting polymers such as PPy [20], PEDOT [21], PProDOT-Et_2 [22] and PANI [23], as well as inorganic compounds such as metal nitrides [24], carbides [25], sulfides [26–28], selenides [29], phosphides [30] and oxides [31] have good electrocatalytic properties as counter materials to replace platinum. However, it is usually not easy to simultaneously reach satisfied optical transparency and electrochemical

* Corresponding authors.
E-mail addresses: guoranli@nankai.edu.cn (G. Li), xpgao@nankai.edu.cn (X. Gao).

http://dx.doi.org/10.1016/j.jpowsour.2014.05.062
0378-7753/

activities [32–35]. Based on the requirement of material science, high transparency demands a film as thin as possible for decreasing reflection and absorption of visible light, while high electrocatalytic activity usually depends on a thick enough film providing abundant active sites [32,35]. In respect of charge transport, a compact electrode film is beneficial for electron transport, but against ion diffusion, vice versa. Therefore, an effective strategy is needed to reach a balance among transparency, electrical conductivity, and electrocatalytic activity.

Non-platinum counter electrodes, made by the doctor-blade method, usually have a thickness with micrometer scale and a loose structure [24–27]. Such electrodes are entirely opaque, and the electrochemical performance mostly is not a patch on platinum. Some transparent non-platinum electrodes such as carbon materials [32,36,37], polyaniline [33], polyrrole [38,39], and metal sulfides [40–43] have been investigated. The film thickness of the transparent electrodes usually is in the range of nanometers. To obtain such a thin film, solution, suspension, and CVD processes seem to be effective. For example, the carbon-based materials can be dispersed into solvents to form a suspension, and then a thin film is obtained by volatilization [32,36]. Based on APCVD method, few-layer graphene films can be fabricated on SiO_2 substrates [44]. A transparent polymer film with the thickness of about 250 nm can be formed on conductive glass by an *in situ* polymerization process [33,38]. An electrodeposition can also make a transparent nickel sulfide film [40]. It provides an inspiration to prepare inorganic compound films directly by the object compounds involved chemical or electrochemical reactions. In addition, it has been also found that some inorganic compounds, such as metal nitrides or sulfides, provide higher intrinsic electrocatalytic activity for reduction of triiodine ions than carbon materials [24,26]. Within the thickness limitation from transparency available, the inorganic compound film electrodes have more chances to achieve or exceed the platinum level.

Herein, a new strategy is proposed to prepare transparent counter electrodes with Group VIIIB metal sulfides for DSSCs. The preparation processes, optical and electrochemical properties, and photoelectrochemical performance of the sulfide counter electrodes are analyzed and discussed based on the requirement for the balance between optical transparency and electrochemical activity.

2. Experimental

2.1. Preparation of metal sulfide electrodes

$Ni(CH_3COO)_2{\cdot}4H_2O$ (1 mmol), 1-octadecene (20 mL), and oleic acid (3 mL) were added into a round flask (50 mL) in sequence. The mixture solution was then heated under vacuum at 90 °C for 3 h. The flask was flushed with nitrogen for 30 min in a distillation set-up, and then the temperature was raised to 200 °C. 1-dodecanethiol (3 mL) was injected into the flask by injector immediately, and the temperature was maintained at 180 °C for 40 min. At room temperature, hexane (20 mL) was used to dilute the resulting mixture, and then ethanol (40 mL) were added to flocculate the product. The solid product were separated by centrifugation, washed using the mixed n-hexane and ethanol (1:4), and dried under vacuum at 70 °C for 12 h. The solid product could be dissolved into hexane (10 mg mL^{-1}) to prepare transparent electrodes. In the case of cobalt sulfide, cobalt acetylacetonate and oleyl amine were used to replace nickel acetic and 1-octadecene, respectively, and the other steps were similar to the above procedure. To prepare iron sulfide, iron (III) acetylacetonate was used as starting material.

To prepare electrodes, a clean FTO (fluorine-doped SnO_2) glass substrate (1.0 × 2.0 cm^2) with a hole (15 $\Omega\square^{-1}$, Nippon Sheet Glass) was first dried in an oven at 140 °C overnight. Different amount of the solutions were spun onto the substrate at 5000 rpm using a WS-400B-6NPP-Lite single wafer spin processor. Finally, the metal sulfide electrodes were obtained after the calcination at different temperature (300 °C for nickel sulfide, 350 °C for cobalt sulfide and 400 °C for iron sulfide) for 1 h under an Ar flow. As reference sample, a platinum electrode was obtained by the pyrolysis of H_2PtCl_6 terpilenol solution at 400 °C for 30 min.

2.2. Fabrication of solar cells

The photoanode was prepared by the same process of our previous works [41]. The electrolyte was composed of I_2 (0.05 mol L^{-1}), LiI (0.1 mol L^{-1}), 1,2-dimethyl-3-propylimidazolium iodide (DMPII, 0.6 mol L^{-1}), and 4-tert-butyl pyridine (TBP, 0.5 mol L^{-1}), with acetonitrile as the solvent. Hot-melt Surlyn film was used to separated the photoanode and the counter electrode, and the electrolyte was injected into the interspace through the hole on the counter electrode under vacuum. Finally, the hole was sealed with a Surlyn film covered with a thin glass slide under heat. The effective cell area of photoanode was 0.2 cm^2.

2.3. Characterization

The structure and morphology of the as-prepared materials or electrodes were examined by X-ray diffraction (XRD, Rigaku MiniFlex II), transmission electron microscopy (TEM, FEI Tecnai F20, equipped with an energy-dispersive X-ray spectrometer), and scanning electron microscopy (SEM, Hitachi S-4800, equipped with an energy-dispersive X-ray spectrometer). The absorption spectra of the counter-electrodes were recorded by a UV–Visible spectrophotometer (CARY 100) with the bare FTO glass absorption as the baseline.

2.4. Electrochemical measurements

Photocurrent density–voltage (*J–V*) characteristic curves, cyclic voltammetry (CV), and electrochemical impedance spectra (EIS) of counter electrodes were recorded using an IM6ex (Zahner) electrochemical workstation. In *J–V* measurement, DSSCs with different counter electrodes were illuminated by a solar simulator (Oriel Sol 2A, Newport) under 100 mW cm^{-2} irradiation, calibrated by a standard silicon solar cell (Oriel Instrument). In CV measurement, a conventional three-electrode system, in which the metal sulfide electrodes or Pt/FTO were used as working electrode, Pt foil as a counter electrode, and Ag/Ag^+ in acetonitrile as a reference electrode, was used in acetonitrile solution containing 10 mmol L^{-1} LiI, 0.1 mol L^{-1} I_2 and 1 mmol L^{-1} $LiClO_4$. The scan range was from 900 mV to −900 mV with a scan rate of 50 mV s^{-1}. EIS spectra were measured in a symmetric cell configuration with two identical counter electrodes, assembled using the same procedure described above with the apparent surface area of 0.38 cm^2. The frequency range was from 100 kHz to 100 mHz with an AC modulation signal of 10 mV and bias DC voltage of −0.60 V.

3. Results and discussion

3.1. Characterization of electrodes

Scheme 1 shows the preparation process of the transparent electrodes assembled with typical nickel sulfide nanoparticles. In the first step, oleic acid groups replace the position of acetic acid groups to generate nickel oleate which can be entirely solved in 1-octadecene at the high temperature. When 1-dodecanethiol is injected into the nickel oleate solution, an alcoholysis process will

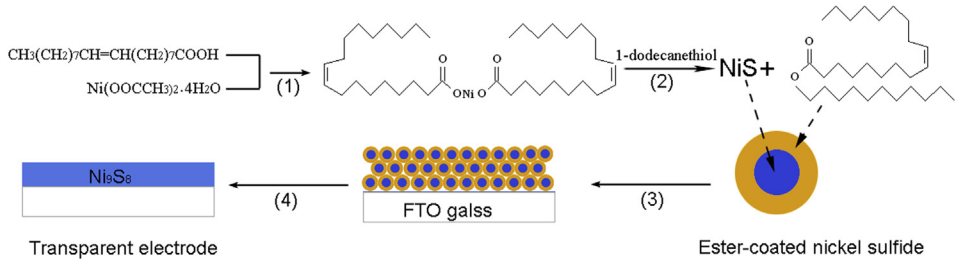

Scheme 1. Schematic preparation process of transparent nickel sulfide electrodes: (1) dissolution, (2) alcoholysis, (3) spin coating, (4) calcination.

occur under the acid condition to form stable nickel sulfide and ester (Step 2). The ester is subject to coating on nickel sulphide due to existence of the long organic chains. The ester-coated nickel sulfide solid can be obtained by extraction with ethanol [45,46]. After spin coating (Step 3) on FTO glass and subsequent calcination (Step 4), the final transparent electrode is obtained. Hereinto, the generation of ester-coated nickel sulfide is crucial for obtaining transparent and high-efficient counter electrodes. Firstly, the ester coating can effectively limit nickel sulfide grains to a small size of about 10 nm. The small grains are subjected to provide high electrocatalytic activity owing to the large surface area. On the other hand, the ester coating is beneficial for the sulfide to dissolve in nonpolar solvents to obtain a precursor solution for films. Besides, the ester coating layer itself will transform into carbon, highly dispersed among nickel sulfide grains after the subsequent heat treatment, which is helpful for improving electrical conductivity of films. The intermediate products in the process are determined by XRD, TG/DSC, Raman, SEM and TEM (Supporting Information Fig. S1). In XRD patterns, the nickel sulfide precursor show many strong diffraction peaks in the relatively low angel range which are generally indexed to organic matter with aliphatic carbon chains. The final nickel sulfide sample presents a stable crystalline phase Ni_9S_8. The relatively low diffraction intensity indicates small sized grains or poor crystallization. The diffraction peaks from the organic components in the precursor disappear after the calcination process. Clearly, TEM observation of the two samples before and after the calcination demonstrates that the nickel sulfide precursor is comprised of organic matter coated nickel sulfide particles based on the mass-thickness contrast (Fig. S1e). TG/DSC curves illustrate that the organic components are decomposed and ejected at the temperature range from 250 to 290 °C, resulting in the weight loss of 79.1%. Thus, a heat treatment at 300 °C is used to obtain nickel sulfide electrodes in the preparation process. The obtained metal sulfide comprises nanosized aggregates, as shown by SEM (Fig. S1d). In detail, TEM observation indicates that the nickel sulfide has sphere-like grains with an average diameter of about 10 nm. The clear interference fringe spacing of the grains declares that the nickel sulfide sample primarily consists of nanocrystals with a good crystallization (Fig. S1f). Usually, the route from organic precursor to inorganic solid is subjected to form a carbon-contained product due to inevitable carbonization in the decomposition of organic components [47]. In this case, involving of carbon is obviously demonstrated by the raising D and G band centered at 1349 and 1593 cm^{-1}, respectively, in Raman spectra of nickel sulfide (Fig. S1c). Furthermore, the relatively strong G band indicates that the carbon contained in nickel sulfides has been graphitized to a large extent [48]. The cases of cobalt and iron sulfides show similar results, as given in Fig. S2. The obtained cobalt sulfide, determined as Co_9S_8, presents a plate-like morphology with a size of several tens nanometers, while the final iron sulfide (FeS) exists as irregular particles from several tens to several hundreds nanometers.

For a film electrode, essential parameters and quality of the active film determine its functional performance. SEM images of a representative nickel sulfide film electrode are exhibited in Fig. 1. In the SEM operation, the high energy electron beam can easily penetrate through the thin film, as a result, the film electrode shows a similar surface image to blank FTO glass (Fig. 1a and b). The cross-section image shows that the active film has the thickness of 100 nm with good uniformity and high-quality compaction. Elemental mapping of the film surface (Fig. 1d) shows that not only nickel and sulfur but also carbon element are uniformly distributed in the active film, in response to the results from Raman spectra (Fig. S1c). According to the EDS result, the carbon amount is about 12.6 at% in the nickel sulfide sample. The uniform carbon distribution is highly positive for the sulfide counter electrode with improving electrical conductivity of the film [49–51]. Besides, carbon is also active for electrochemically catalyzing reduction of triiodine ions [11,12,49–51]. For comparison, SEM surface and cross-section images of platinum electrode with the thickness of 60 nm are shown in Fig. S3.

3.2. Optical transparency of electrodes

The thickness of the electrode films can easily be controlled by varying the dosage of the precursor solution in the spin coating procedure. Apparently, the thickness is an increasing linear function of the precursor solution dosage (Fig. 2 inset). Fig. S4 shows the SEM images of nickel sulfide electrodes with the thickness of 50 nm and 170 nm. The films with different thickness generally have goodish transparency, the transmittance in visible light region being higher than 75% (Fig. 2). As expected, the transparency of the films regularly decreases with increasing the film thickness. Using light transmittance at 500 nm as example, it is a typical decreasing linear function of the thickness of the nickel sulfide films (Fig. 2 inset). SEM images of cobalt and iron sulfides with different thickness are also presented in Figs. S5 and S6. Different from nickel and iron sulfides electrodes, cobalt sulfide aggregate seriously on FTO glass. Light transmittance spectra of the cobalt and iron sulfide films with various thicknesses are given in Fig. S7. With increasing the thickness, transmittance of cobalt sulfide films decreases more obviously as compared with nickel sulfide films, while transmittance of iron sulfide films hardly varies with increasing the thickness.

3.3. Electrochemical property of electrodes

In respect of electrochemical properties of the sulfide electrodes, electrical conductivity and electrocatalytic activity should be concerned simultaneously. The sheet resistance of the sulfide electrodes is measured by the four-point probe method, and electrochemical performance is investigated by cyclic voltammetry measurements and electrochemical impedance spectra. The CV curves of the Pt electrode is similar to our previous work [49,50], where the cathodic peak at about −0.5 V represents the reduction

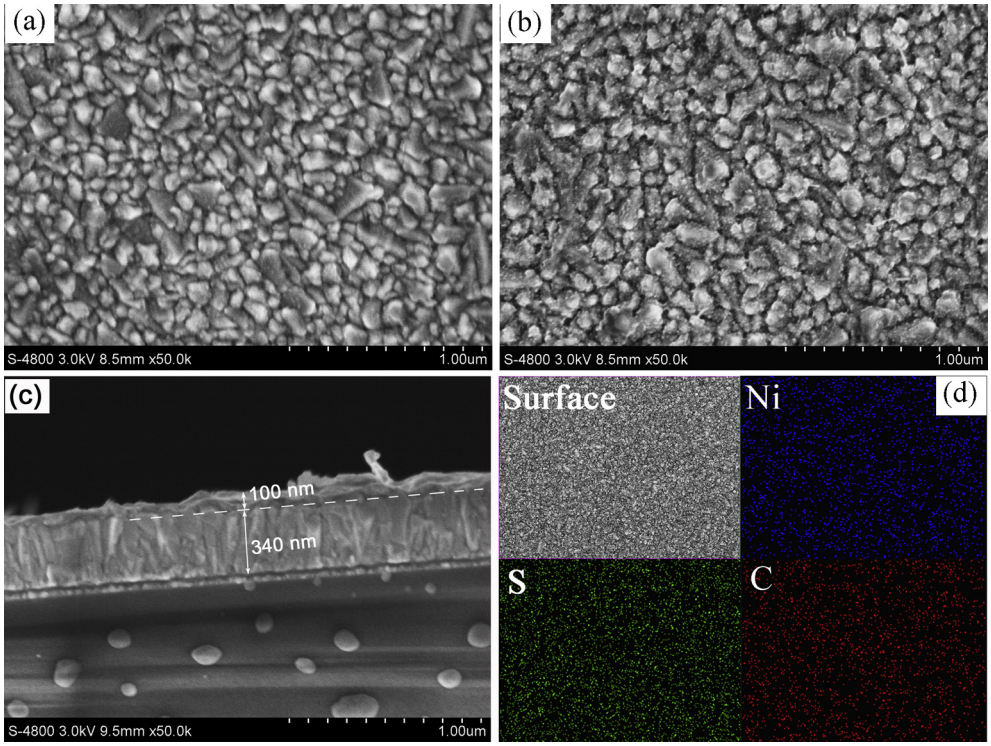

Fig. 1. Surface SEM images of (a) FTO glass and (b) nickel sulfide film; (c) cross-section SEM image and (d) EDS mapping on the top surface of a nickel sulfide film.

of triiodide to iodide (Fig. 3). In the case of NiS100, the cathodic peak has the same position as that for the Pt electrode, suggesting a similar electrocatalytic process on the both electrodes. Notably, NiS100 shows a larger current density than the Pt electrode, illuminating a higher electrocatalytic activity for reduction of triiodide ions. For NiS50 electrode, the relatively low current density for the cathodic process means a slightly low activity as it has a thinner active film. In regard to NiS170, the position of the cathodic peak obviously shift to negative potential. The phenomenon demonstrates that too thick size of active film can depress electrocatalytic activity for reduction of triiodide ions [49,50]. Charge transfer resistance (R_{ct}) and Nernst diffusion impedance (Z_w) can be estimated by simulating EIS spectra according to the equivalent circuit in Fig. 4a. In this case, R_{ct} is mainly related to the electrocatalytic activity for reduction of triiodine ions, and a low R_{ct} value indicates high electrocatalytic activity. Z_w responses ion diffusion and a low Z_w indicates fast ion transport in the electrode–electrolyte interface [49,51]. The simulated data are summarized in Table S1. As shown in Fig. 4b, the sheet resistance of the nickel sulfide films raises monotonously with increasing sulfide film thickness due to semiconductor nature of the metal sulfides. The result reveals that metal sulfide films should be made as thin as possible without concerning the catalysis. R_{ct} presents a non-monotonous variation with increasing the thickness of nickel sulfide films, and the electrode with the thickness of 100 nm has the minimum R_{ct}. As known well, the charge transfer resistance

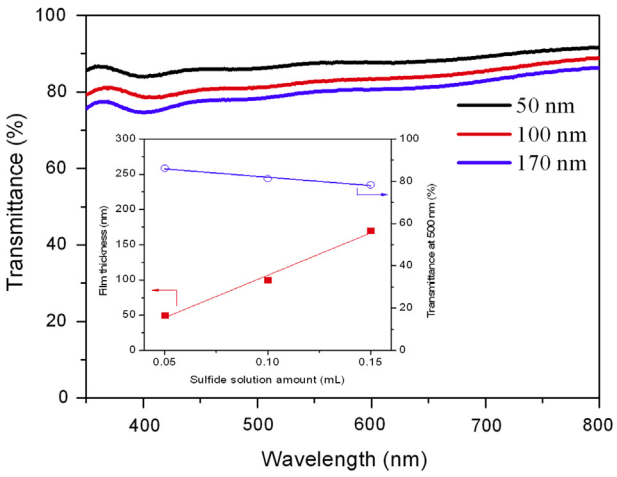

Fig. 2. Transmittance spectra in visible light area of nickel sulfide films with various thicknesses and functions of nickel sulfide films thickness and transmittance at 500 nm with dosage of the precursor solution (the inset).

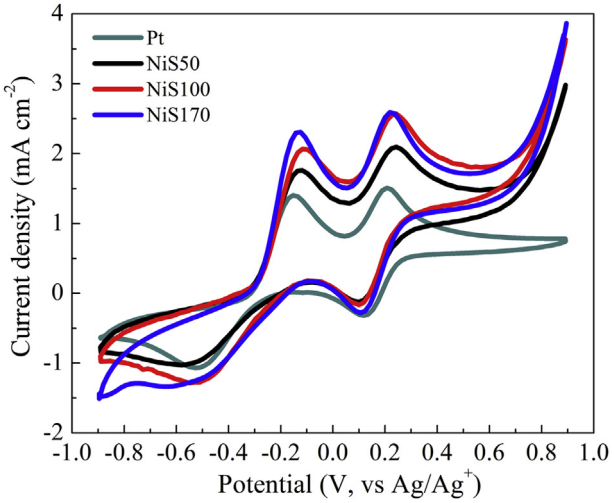

Fig. 3. Cyclic voltammetry measurements of nickel sulfide electrodes with different thickness and Pt electrode.

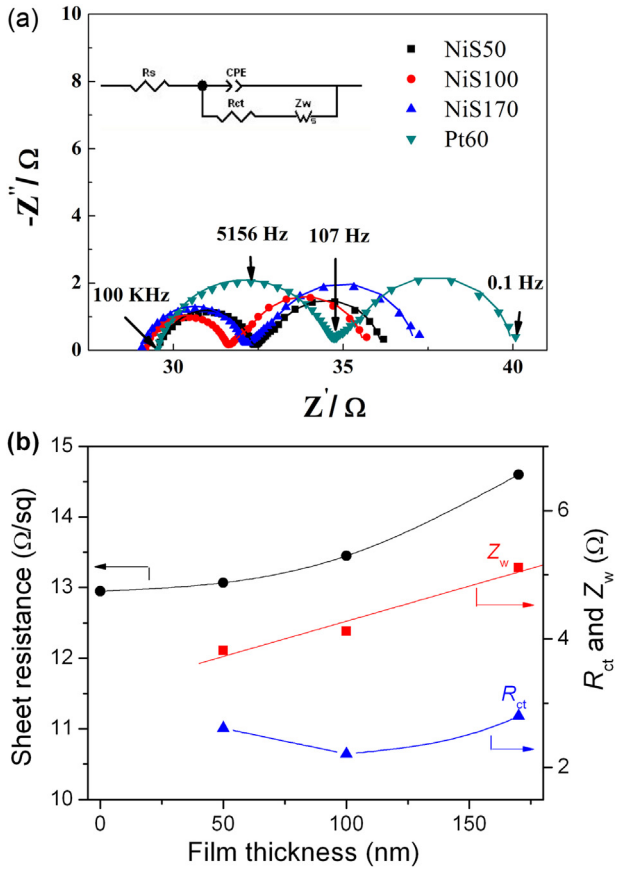

Fig. 4. (a) Nyquist plots of the symmetric cells with two identical counter electrodes of nickel sulfides or platinum. The symbols and lines correspond to the experimental and simulated data, respectively. The cells were measured with the frequency range of 100 KHz–100 mHz. In the equivalent circuit, R_{ct}: charge-transfer resistance; Z_W: Nernst diffusion impedance; R_s: series resistance; *CPE*: constant phase element (the number indicates its thickness with nanometer unit). (b) functions of sheet resistance, charge transfer resistance (R_{ct}) and diffusion impedance (Z_w) with nickel sulfide film thicknesses.

depends highly on nature of electrode material and actual electroactive area of electrode [51]. A too thin film can not ensure enough active sites for reduction of triiodine ions, while a thick film is not always favorable, because the efficient thickness of a porous electrode is actually restricted by electron distribution and electrolyte penetration in porous film [52]. Furthermore, as mentioned above, the thicker the electrode film, the higher the sheet resistance. Therefore, the thickness of 100 nm is the reasonable trade-off among the above factors for the nickel sulfide film. With regards to Z_W, there is a linear function with increasing the thickness of nickel sulfide films. This suggests that the increase of the thickness is unfavorable for ion diffusion in the compact nickel sulfide films.

The iron sulfide films show a similar change in the electrochemical parameters with increasing the thickness as the nickel sulfide films (Fig. S8 and Table S1). However, cobalt sulfide films present an unusual phenomenon that R_{ct} decreases monotonously with increasing the thickness to 380 nm. Unfortunately, the cobalt sulfide film with the thickness of 380 nm has only 50% light transmittance (Fig. S7). Since transparency is highly concerned in this work, the thicker cobalt sulfide films are not discussed here.

3.4. Photovoltaic performance

Fig. 5a shows the characteristic *J–V* curves of the DSSCs using transparent nickel sulfide counter electrodes with various film thicknesses, as well as the platinum electrode as reference. The detailed photovoltaic parameters from *J–V* curves are listed in Table S2. Noticeably, the energy conversion efficiency (η, 7.37%) of the DSSC using the nickel sulfide counter electrode with the thickness of 100 nm (denoted as NiS100), is slightly higher than that (7.20%) of the device using the conventional Pt counter electrode. A comparison in detail shows that the short circuit current (J_{sc}) is dominant for improving the energy conversion efficiency of the corresponding device with NiS100, resulting mainly from relatively a fast electrode kinetics process and low polarization. As shown in Fig. 4, NiS100 has the lowest charge transfer resistance and the small diffusion impedance, demonstrating its advantage on electrode kinetics. On the other hand, the polarization in this case includes both ohmic polarization and electrochemical polarization. Ohmic polarization is derived from ohmic resistance of the electrodes. With increasing thickness, the sulfide films have increasing resistance as shown in Fig. 4b. This means that ohmic polarization increases with an increase in thickness. Electrochemical polarization occurs at the electrode–electrolyte interface, which is related to electrocatalytic activity and triiodide ion diffusion in mass transport networks of the sulfide electrodes. A low electrocatalytic activity and slow ion

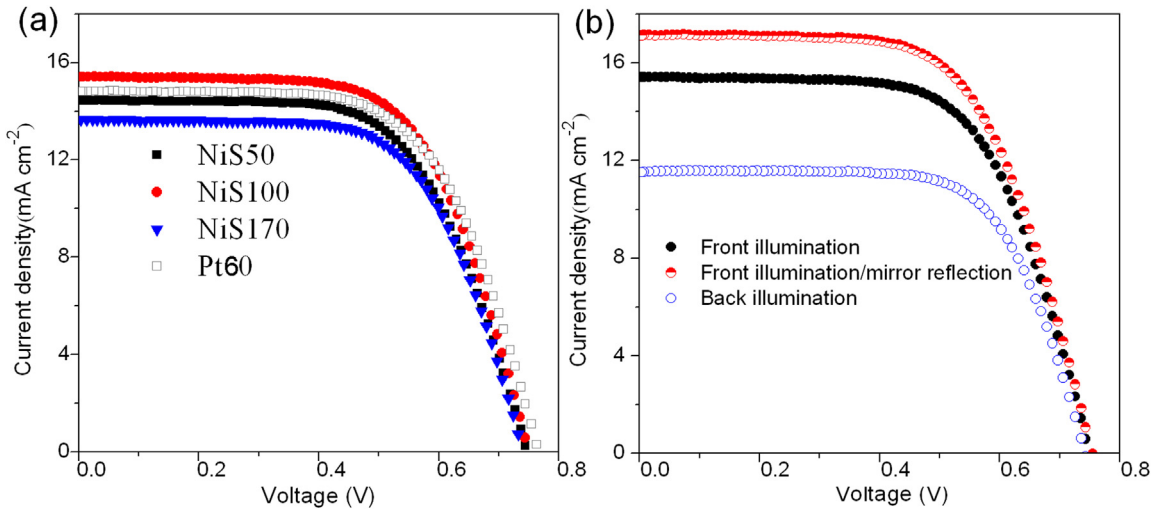

Fig. 5. Characteristic *J–V* curves of DSSCs (a) using transparent nickel sulfide electrodes with different thicknesses and platinum electrode with a thickness of 60 nm, and (b) using NiS100 under different illumination models.

diffusion will induce electron accumulation to form electrochemical polarization. This will further influence electric double-layer distribution to depress diffusion of triiodide anion. As a result, electrochemical polarization is unfavorable for improving current density and voltage of DSSCs. NiS170 has a relatively high charge transfer resistance, sheet resistance and diffusion impedance, meaning a higher ohmic polarization and electrochemical polarization. Consequentially the low short circuit current and open circuit voltage can be observed in Fig. 5. In the case of the NiS50 electrode, the short circuit current (J_{sc}) is slightly lower as compared with those of the NiS100 electrode, which is attributed to the relatively low electroactive area in the thin nickel sulfide film. The similar phenomena are also found in the tests of the iron sulfide electrodes. The iron sulfide film with the moderate thickness of 100 nm shows the optimized electrochemical performance. Without regards to transparency, the cobalt sulfide film with the thickness of 380 nm is the best one according to the evaluation of the electrochemical performance. Therefore, nickel sulfide is the better choice than cobalt and iron sulfides in view of optical transparency and electrochemical performance (Fig. S7 and Table S2).

The use of the transparent counter electrodes is energetically favorable for the corresponding DSSCs to work under different illumination conditions. Fig. 5b shows the characteristic *J*–*V* curves of the DSSC using NiS100 tested with a reflecting mirror behind the counter electrode (Front illumination-mirror reflection) or with illumination from the backside of the counter electrode (Back illumination). Under the condition of "front illumination-mirror reflection", the light permeated into the DSSC is reflected by the plane mirror into TiO_2 photoanode again to excite photo-generated electrons, which increases the final energy conversion efficiency from 7.37% to 8.11%. The "back illumination" test more directly verifies the advantage of the transparent counter electrode, where the energy conversion efficiency of 5.80% is reached. The results confirm the advantages of the transparent counter electrode in DSSCs, which undoubtedly provides more room for the development of DSSCs.

4. Conclusion

In conclusion, the transparent counter electrodes with Group VIIIB metal sulfides are prepared by the organic solution route. The thickness of the metal sulfide films can be controllably adjusted in the range of several hundreds of nanometers. Transparency of the sulfide films decrease monotonously with increasing the thickness. The sheet resistance and Nernst diffusion impedance of the sulfide films increase monotonously with increasing the thickness. However, the charge transfer resistance for reduction of triiodine ions has a minimum in a certain film thickness, leading to the optimized photoelectrochemical performance. As counter electrode, the nickel sulfide film with the thickness of 100 nm shows the high transparency and energy conversion efficiency of 7.37%, higher than that of the DSSC using platinum electrode. The results declare that the strategy for preparing metal sulfide counter electrodes can realize the balance between optical transparency and electrochemical performance.

Acknowledgments

The financial support from the NSFC (51001063), the Natural Science Foundation of Tianjin (12JCQNJC00700) and MOE Innovation Team (IRT13022) are greatly appreciated.

Appendix A. Supplementary data

Supplementary data related to this article can be found at http://dx.doi.org/10.1016/j.jpowsour.2014.05.062.

References

[1] N.G. Park, K. Kim, Phys. Stat. Sol.(A) 205 (2008) 1895–1904.
[2] B. O'Regan, M. Grätzel, Nature 353 (1991) 737–740.
[3] Z.J. Ning, Y. Fu, H. Tian, Energy Environ. Sci. 3 (2010) 1170–1181.
[4] S. Yoon, S. Tak, J. Kim, Y. Jun, K. Kang, J. Park, Build. Environ. 46 (2011) 1899–1904.
[5] S.F. Zhang, X.D. Yang, Y. Numata, L.Y. Han, Energy Environ. Sci. 6 (2013) 1443–1464.
[6] X. Fan, Z.Z. Chu, L. Chen, C. Zhang, F.Z. Wang, Y.W. Tang, J.L. Sun, D.C. Zou, Appl. Phys. Lett. 92 (2008) 113510.
[7] G. Calogero, P. Calandra, A. Irrera, A. Sinopoli, I. Citro, G.D. Marco, Energy Environ. Sci. 4 (2011) 1838–1844.
[8] N. Papageorgiou, Coord. Chem. Rev. 248 (2004) 1421–1446.
[9] F. Hao, P. Dong, Q. Luo, J.B. Li, J. Lou, H. Lin, Energy Environ. Sci. 6 (2013) 2003–2019.
[10] T.N. Murakami, M. Grätzel, Inorg. Chim. Acta 361 (2008) 572–580.
[11] P. Joshi, Y. Xie, M. Ropp, D. Galipeau, S. Bailey, Q.Q. Qiao, Energy Environ. Sci. 2 (2009) 426–429.
[12] J.K. Chen, K.X. Li, Y.H. Luo, X.Z. Guo, D.M. Li, M.H. Deng, S.Q. Huang, Q.B. Meng, Carbon 47 (2009) 2704–2708.
[13] L.H. Chang, C.K. Hsieh, M.C. Hsiao, J.C. Chiang, P.I. Liu, K.K. Ho, C.M. Ma, M.Y. Yen, M.C. Tsai, C.H. Tsai, J. Power Sources 222 (2013) 518–525.
[14] M.X. Wu, X. Lin, T.H. Wang, J.S. Qiu, T.L. Ma, Energy Environ. Sci. 4 (2011) 2308–2315.
[15] W.W. Sun, X.H. Sun, T. Peng, Y.M. Liu, H.W. Zhu, S.S. Guo, X.Z. Zhao, J. Power Sources 201 (2012) 402–407.
[16] W. Zeng, G.J. Fang, T.Y. Han, B.R. Li, N.S. Liu, D.S. Zhao, Z.Q. Liu, D.Y. Wang, X.Z. Zhao, D.C. Zou, J. Power Sources 245 (2014) 456–462.
[17] W. Zeng, G.J. Fang, B.R. Li, Z.Q. Liu, T.Y. Han, J. Wang, F.W. Liu, P.F. Fang, X.Z. Zhao, D.C. Zou, ACS Appl. Mater. Interf. 5 (2013) 7101–7108.
[18] S.C. Hou, X. Cai, Y.P. Fu, Z.B. Lv, D. Wang, H.W. Wu, C. Zhang, Z.Z. Chu, D.C. Zou, J. Mater. Chem. 21 (2011) 13776–13779.
[19] S.C. Hou, X. Cai, H.W. Wu, Z.B. Lv, D. Wang, Y.P. Fu, D.C. Zou, J. Power Sources 215 (2012) 164–169.
[20] J.H. Wu, Q.H. Li, L.Q. Fan, Z. Lan, P.J. Li, J.M. Lin, S.C. Hao, J. Power Sources 181 (2008) 172–176.
[21] J.M. Pringle, V. Armel, D.R. Macfarlane, Chem. Commun. 46 (2010) 5367–5369.
[22] K.M. Lee, P.Y. Chen, C.Y. Hsu, J.H. Huang, W.H. Ho, H.C. Chen, K.C. Ho, J. Power Sources 188 (2009) 313–318.
[23] Q.H. Li, J.H. Wu, Q.W. Tang, Z. Lan, P.J. Li, J.M. Lin, L.Q. Fan, Electrochem. Commun. 10 (2008) 1299–1302.
[24] G.R. Li, J. Song, G.L. Pan, X.P. Gao, Energy Environ. Sci. 4 (2011) 1680–1683.
[25] M.X. Wu, X.A. Lin, A. Hagfeldt, T.L. Ma, Angew. Chem. Int. Ed. 50 (2011) 3520–3524.
[26] M.K. Wang, A.M. Anghel, B. Marsan, N.C. Ha, N. Pootrakulchote, S.M. Zakeeruddin, M. Grätzel, J. Am. Chem. Soc. 131 (2009) 15976–15977.
[27] Y.Y. Dou, G.R. Li, J. Song, X.P. Gao, Phys. Chem. Chem. Phys. 14 (2012) 1339–1342.
[28] H.C. Sun, D. Qin, S.Q. Huang, X.Z. Guo, D.M. Li, Y.H. Luo, Q.B. Meng, Energy Environ. Sci. 4 (2011) 2630–2637.
[29] H.J. Chen, Y. Xie, H.L. Cui, W. Zhao, X.L. Zhu, Y.M. Wang, X.J. Lü, F.Q. Huang, Chem. Commun. 50 (2014) 4475–4477.
[30] W. Zhao, X.L. Zhu, H. Bi, H.L. Cui, S.R. Sun, F.Q. Huang, J. Power Sources 242 (2013) 28–32.
[31] M.X. Wu, X. Lin, Y.D. Wang, L. Wang, W. Guo, D.D. Qu, X.J. Peng, A. Hagfeldt, M. Grätzel, T.L. Ma, J. Am. Chem. Soc. 134 (2012) 3419–3428.
[32] L. Kavan, J.H. Yum, M. Grätzel, ACS Nano 5 (2011) 165–172.
[33] Q.D. Tai, B.L. Chen, F. Guo, S. Xu, H. Hu, B. Sebo, X.Z. Zhao, ACS Nano 5 (2011) 3795–3799.
[34] S.S. Jeon, C. Kim, T.H. Lee, Y.W. Lee, K. Do, J. Ko, S.S. Im, J. Phys. Chem. C. 116 (2012) 22743–22748.
[35] P. Kuang, J.M. Park, W. Leung, R.C. Mahadevapuram, K.S. Nalwa, T.G. Kim, S. Chaudhary, K.M. Ho, K. Constant, Adv. Mater. 23 (2011) 2469–2473.
[36] J.E. Trancik, S.C. Braton, J. Hone, Nano Lett. 8 (2008) 982–987.
[37] C.H. Bu, Y.M. Liu, Z.H. Yu, S.J. You, N. Huang, L.L. Liang, X.Z. Zhao, ACS Appl. Mater. Interf. 5 (2013) 7432–7438.
[38] C.H. Bu, Q.D. Tai, Y.M. Liu, S.S. Guo, X.Z. Zhao, J. Power Sources 221 (2013) 78–83.
[39] D.K. Hwang, D. Song, S.S. Jeon, T.H. Han, Y.S. Kang, S.S. Im, J. Mater. Chem. A 2 (2014) 859–865.
[40] Z.L. Ku, X. Li, G.H. Liu, H. Wang, Y.G. Rong, M. Xu, L.F. Liu, M. Hu, Y. Yang, H.W. Han, J. Mater. Chem. A 1 (2013) 237–240.
[41] B. Lei, G.R. Li, X.P. Gao, J. Mater. Chem. A 2 (2014) 3919–3925.
[42] F. Gong, H. Wang, X. Xu, G. Zhou, Z.S. Wang, J. Am. Chem. Soc. 134 (2012) 10953–10958.
[43] J.Y. Lin, S.W. Chou, Electrochem. Commun. 37 (2013) 11–14.
[44] H. Bi, S.R. Sun, F.Q. Huang, X.M. Xie, M.H. Jiang, J. Mater. Chem. 22 (2012) 411–416.
[45] W.H. Shi, J.X. Zhu, X.H. Rui, X.H. Cao, C. Chen, H. Zhang, H.H. Hng, Q.Y. Yan, ACS Appl. Mater. Interf. 4 (2012) 2999–3006.
[46] P.T. Zhao, Q.M. Zeng, K.X. Huang, Mater. Lett. 63 (2009) 313–315.
[47] H.M. Wang, W. Li, M.H. Zhang, Chem. Mater. 17 (2005) 3262–3267.

[48] A.C. Ferrari, J.C. Meyer, V. Scardaci, C. Casiraghi, M. Lazzeri, F. Mauri, S. Piscanec, D. Jiang, K.S. Novoselov, S. Roth, A.K. Geim, Phys. Rev. Lett. 97 (2006) 187401.
[49] G.R. Li, F. Wang, Q.W. Jiang, X.P. Gao, P.W. Shen, Angew. Chem. Int. Ed. 49 (2010) 3653–3656.
[50] G.R. Li, F. Wang, J. Song, F.Y. Xiong, X.P. Gao, Electrochim. Acta 65 (2012) 216–220.
[51] J. Song, G.R. Li, F.Y. Xiong, X.P. Gao, J. Mater. Chem. 22 (2012) 20580–20585.
[52] C. Punckt, M.A. Pope, J. Liu, Y.H. Lin, I.A. Aksay, Electroanalysis 22 (2010) 2834–2841.